

Local Basis Transformation to Mitigate Negative Sign Problems

Keisuke Murota¹ and Syngae Todo^{1,2,3}

¹*Department of Physics, The University of Tokyo, Tokyo 113-0033, Japan*

²*Institute for Physics of Intelligence, The University of Tokyo, Tokyo 113-0033, Japan*

³*Institute for Solid State Physics, The University of Tokyo, Kashiwa, 277-8581, Japan*

Quantum Monte Carlo (QMC) methods for the frustrated quantum spin systems occasionally suffer from the negative sign problem, which makes simulations exponentially harder for larger systems at lower temperatures and severely limits QMC's application across a wide range of spin systems. This problem is known to depend on the choice of representation basis. We propose a systematic approach for mitigating the sign problem independent of the given Hamiltonian or lattice structure. We first introduce the concept of negativity to characterize the severity of the negative sign problem. We then demonstrate the existence of a locally defined quantity, the L1 adaptive loss function, which effectively approximates negativity, especially in frustration-free systems. Using the proposed loss function, we demonstrate that optimizing the representation basis can mitigate the negative sign. This is evidenced by several frustration-free models and other important quantum spin systems. Furthermore, we compare the effectiveness of unitary transformations against the standard orthogonal transformation and reveal that unitary transformations can effectively mitigate the sign problem in certain cases.

I. INTRODUCTION

Quantum Monte Carlo (QMC) methods are powerful computational tools for studying quantum many-body systems [1–3]. The QMC methods map a d -dimensional quantum system onto a $(d + 1)$ -dimensional classical counterpart via the Suzuki-Trotter decomposition, which allows for the effective simulation of quantum spin systems. The QMC method is particularly advantageous because it can handle large, strongly correlated systems with high computational efficiency, scaling linearly with the number of lattice sites and the inverse temperature in ideal cases.

Among various QMC algorithms, the loop algorithm [4, 5] and its generalization, the worm algorithm [6, 7], are noteworthy. The worm algorithm, in particular, is based on the stochastic series expansion (SSE) [8] and is designed to handle the complexities of quantum spin systems by creating and manipulating loops within the lattice. This method improves the efficiency of sampling configurations and has become a robust, standard approach in QMC simulations.

Despite the advantages of QMC methods, they are significantly hindered by the negative sign problem. To be more specific, in the case of quantum spin systems, the negative sign problem arises when the Hamiltonian matrix involves positive off-diagonal elements. This notorious problem makes the direct application of QMC sampling impossible in many intriguing cases, as the Boltzmann weight becomes negative and can not be interpreted as a (unnormalized) probability. To address this issue, a common strategy is simulating a system with a well-behaved virtual Hamiltonian that closely resembles the original one but has no positive off-diagonal elements and then compensating for the difference through the average sign [9–11]. Approximately, the average sign is given by $\langle S \rangle \propto e^{-\beta \Delta F}$, where β is the inverse temperature and ΔF is the difference in the free energy between

the original and virtual systems. Thus, the sampling efficiency degrades exponentially with the number of lattice sites and the inverse temperature, making simulations increasingly difficult for larger systems at lower temperatures.

So far, several approaches have been explored to alleviate this problem. One approach focuses on the selection of better virtual Hamiltonians. In Refs. 9–11, the authors argued that the condition for good virtual Hamiltonians is that ΔF is small, meaning the average sign $\langle S \rangle$ is close to 1, and the virtual Hamiltonians are constructed based on this strategy. On the other hand, most modern approaches rely on the representation basis dependencies of the negative sign problem and try to find a negative-sign-free basis for conducting QMC simulations [12–22]. Actually, there are several known examples that completely cure the negative sign problem with this approach, including canonical cluster basis [23], and dimer-like basis rotations [16–20, 23–26]. Although these methods can eliminate the negative sign problem, they are model-specific and rely on physical intuition to construct the negative-sign-free basis, making them difficult to formulate systematically. In response to these issues, the current trend is to systematically mitigate the negative sign by optimizing local orthogonal basis transformation with respect to certain loss functions [12, 15, 21, 22]. These approaches take full advantage of computational power, offering the benefit of reducing the negative sign problem without restricting the target physical systems.

In this paper, we first introduce the concept of “negativity” to characterize the severity of the negative sign problem and formulate the optimization problem of the negative sign using this negativity as a loss function. By analyzing this quantity, we show that the conventional strategy for choosing the virtual Hamiltonian, that is, simply using the absolute value of the weight of the original Hamiltonian, is always the best in this formulation, reducing the problem to simply the optimization of the

representation basis. Ideally, there should be no constraints on the basis transformation, but practically, the transformation matrix should be limited to those represented as a product of local transformations. Otherwise, the optimization becomes infeasible. Therefore, in the latter part, we discuss approaches to optimize local transformations using the negativity as the loss function.

In particular, we introduce the *L1 adaptive loss function* as a computationally efficient approximation of the negativity to optimize the local basis instead of directly optimizing the negativity itself, which is computationally intractable. We also show that the L1 adaptive loss function approximates the negativity well in so-called *frustration-free* quantum spin systems and gives an upper bound. This fact highlights the importance of the frustration-free property in mitigating the negative sign problem, as seen in the fact that most of the known quantum spin systems with negative-sign-free basis become frustration-free in some parameter regime [17–20, 24].¹

Most previous studies on local basis transformations have focused only on orthogonal transformations. However, unitary transformations can also be utilized in QMC methods. In this study, we also explore whether unitary transformations have the potential to mitigate the negative sign problem further.

The outline of this paper is as follows: In Section II, we review the negative sign problem in the QMC methods and the cause of the negative sign problem. In Section III, we discuss quantifying the negative sign problem by introducing the concept of negativity. In Section IV, we introduce the L1 adaptive loss function as a good approximation of the negativity and discuss the optimization problem of the local basis transformation using this quantity. In Section V, we present numerical results demonstrating the effectiveness of our approach on the frustration-free quantum spin models as well as for the various non-frustration-free models. After that, in Section VI, we compare the performance of the orthogonal and unitary transformations. Finally, in Section VII, we summarize our findings and potential directions for future research.

II. QUANTUM MONTE CARLO WITH NEGATIVE WEIGHT

First, we review the QMC method and the conventional approach when the Hamiltonian contains positive off-diagonal elements. In the formalism of SSE, the partition function is calculated by summing weights of all possible configurations of the extended $(d + 1)$ -dimensional classical system. Let's assume our system Hamiltonian can be expressed as $H = \sum_{b \in \mathcal{B}} h_b$. Here, h_b is a local

Hamiltonian acting on a single bond b , and \mathcal{B} is the set of all bonds in the system. In the following, we use $G \equiv -H$ and $g_b \equiv -h_b$ for $b \in \mathcal{B}$ to simplify the notation. Then, the partition function is represented as

$$\begin{aligned} Z &= \text{Tr} [\exp(\beta G)] \approx \sum_{\psi_1} \langle \psi_1 | \prod_{k=1}^M (1 + \frac{\beta}{M} G) | \psi_1 \rangle \\ &= \sum_{\{\psi_k\}} \langle \psi_1 | (1 + \frac{\beta}{M} G) | \psi_2 \rangle \cdots \langle \psi_M | (1 + \frac{\beta}{M} G) | \psi_1 \rangle \\ &= \sum_{\{\psi_k\}} \sum_{\{b_k\}} \langle \psi_1 | (1 + \frac{\beta}{M} g_{b_1}) | \psi_2 \rangle \cdots \\ &\quad \times \langle \psi_M | (1 + \frac{\beta}{M} g_{b_M}) | \psi_1 \rangle. \end{aligned} \quad (1)$$

Here, $|\psi\rangle$ is the basis of the Hilbert space of the system and the collections of states and bonds, ψ_1, \dots, ψ_M and b_1, \dots, b_M , define a single configuration of the system, c_M . Note that in the actual QMC simulation, we can rigorously take the infinite M limit, and the simulation becomes unbiased, thus, we will express the configuration without the label M to indicate the infinite M limit in the following. Finally, by expressing the weight of a configuration c as $W(c)$, we can write the partition function as the sum of weights of all configurations:

$$Z = \sum_{c \in \mathcal{C}} W(c). \quad (2)$$

Here, \mathcal{C} is the set of all configurations of the system.

Usually, with above definition of $W(c)$, the expectation of an observable \mathcal{O} can be expressed as

$$\langle \mathcal{O} \rangle = \frac{1}{Z} \sum_{c \in \mathcal{C}} W(c) \mathcal{O}(c). \quad (3)$$

In QMC, Eq. (3) is interpreted as sample average over distribution $W(c)/\sum_{c \in \mathcal{C}} W(c)$ as long as all weights are non-negative. On the flip side, the situation becomes exponentially more complex in the case of $W(c)$ taking negative values. In this case, $W(c)/Z$ cannot be regarded as a probability distribution, and the so-called reweighting approach is used as a workaround. More concretely, instead of simulating the Hamiltonian G , we simulate a virtual Hamiltonian G_v , where off-diagonal elements are all positive and then reweight the results afterward as follows:

$$\langle \mathcal{O} \rangle = \frac{\sum_{c \in \mathcal{C}} W_v(c) \frac{W(c)}{W_v(c)} \mathcal{O}(c)}{\sum_{c \in \mathcal{C}} W_v(c) \frac{W(c)}{W_v(c)}} = \frac{\langle S\mathcal{O} \rangle_v}{\langle S \rangle_v}. \quad (4)$$

Here, $\langle A \rangle_v$ denotes the expectation value of A evaluated for the virtual Hamiltonian G_v . We also defined the reweighting factor $S(c) = W(c)/W_v(c)$. The expectation value of the reweighting factor is often called the *average sign*.

¹ It should be noted that frustration-free models are not always free of the negative sign problem. The details will be discussed later.

III. QUANTIFICATION OF NEGATIVE SIGN PROBLEM

Simple analytical calculation of the statistical error of the estimator Eq. (4) tells that temperature dependency of the statistical error is fully characterized by the relative error of the average sign, $\eta = \sqrt{\langle |S|^2 \rangle_{\mathbf{v}} / \langle S \rangle_{\mathbf{v}}^2}$. In the following, we call this quantity the *negativity*, and by optimizing η either via basis transformation or choice of a virtual Hamiltonian, we try to mitigate the effect of the negative sign problem. Interestingly, however, as for the choice of the virtual Hamiltonian, we can confirm that the standard choice $G_{\mathbf{v}} = G^+$, the so-called stoquastic of G , where each non-diagonal element in G is replaced by its absolute value, always achieves the optimal negativity as shown in the following proposition:

Proposition 1 (Optimal virtual Hamiltonian). We first express the negativity using the weight $W(c)$ and $W_{\mathbf{v}}(c)$:

$$\begin{aligned} \eta^2 &= \frac{\langle |S|^2 \rangle_{\mathbf{v}}}{|\langle S \rangle_{\mathbf{v}}|^2} = \frac{\sum_{c \in \mathcal{C}} |W(c)|^2 / W_{\mathbf{v}}(c)}{\sum_{c \in \mathcal{C}} W_{\mathbf{v}}(c)} \cdot \frac{\left| \sum_{c \in \mathcal{C}} W_{\mathbf{v}}(c) \right|^2}{\left| \sum_{c \in \mathcal{C}} W(c) \right|^2} \\ &= \frac{\left[\sum_{c \in \mathcal{C}} |W(c)|^2 / W_{\mathbf{v}}(c) \right] \cdot \left[\sum_{c \in \mathcal{C}} W_{\mathbf{v}}(c) \right]}{\left[\sum_{c \in \mathcal{C}} W(c) \right]^2} \\ &\geq \frac{\left[\sum_{c \in \mathcal{C}} \sqrt{|W(c)|^2 / W_{\mathbf{v}}(c)} \cdot \sqrt{W_{\mathbf{v}}(c)} \right]^2}{\left[\sum_{c \in \mathcal{C}} W(c) \right]^2} \\ &= \frac{\left[\sum_{c \in \mathcal{C}} |W(c)| \right]^2}{\left[\sum_{c \in \mathcal{C}} W(c) \right]^2} = \left[\frac{\text{Tr} [\exp(\beta G^+)]}{\text{Tr} [\exp(\beta G)]} \right]^2. \end{aligned} \quad (5)$$

Here, we used the Cauchy-Schwarz inequality between $\sqrt{W_{\mathbf{v}}(c)}$ and $\sqrt{|W(c)|^2 / W_{\mathbf{v}}(c)}$ to obtain inequality from the second line to the third line. We also use $W_{\mathbf{v}}(c) > 0 \forall c$ and $\sum_{c \in \mathcal{C}} W(c) = Z > 0$. The equality on the third line is achieved when $W_{\mathbf{v}}(c) = |W(c)|$, which is equivalent to $G_{\mathbf{v}} = G^+$.

This proposition claims that we do not have to care about the virtual Hamiltonian in the first place. By choosing $G_{\mathbf{v}} = G^+$, the negativity reduces to $\eta = |\langle S \rangle_{\mathbf{v}}|^{-1}$, i.e., the severity of the negative sign problem is characterized by the average sign. Similar discussion is also done in Refs. 12 and 13.

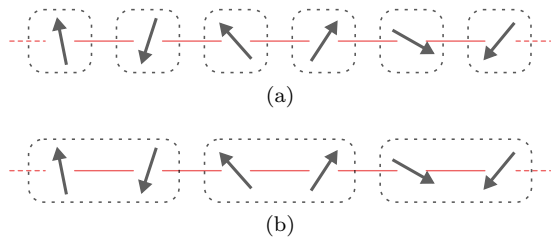


FIG. 1. Illustration of the unitary transformation and the choice of cells for quantum spin chains. Here, we consider two types of cells to which the same local unitary transformation is applied.

IV. LOCAL BASIS TRANSFORMATION

A. Negativity in low temperature limit

When both G and G^+ have unique ground state, the average sign has the following asymptotic form

$$\begin{aligned} \eta &= |\langle S \rangle_{\mathbf{v}}|^{-1} = \frac{\sum_{c \in \mathcal{C}} W_{\mathbf{v}}(c)}{\left| \sum_{c \in \mathcal{C}} W_{\mathbf{v}}(c) \cdot \frac{W(c)}{W_{\mathbf{v}}(c)} \right|} \\ &= \frac{\sum_{c \in \mathcal{C}} W_{\mathbf{v}}(c)}{\sum_{c \in \mathcal{C}} W(c)} \approx e^{\beta(\lambda^+(G) - \lambda(G))} \end{aligned} \quad (6)$$

for large β . Here, $\lambda(G)$ and $\lambda^+(G)$ denote the largest eigenvalue of G and G^+ , respectively. Since the average sign approaches zero exponentially for larger β , it is sometimes more convenient to use $\eta' \equiv \lambda^+(G) - \lambda(G)$ as a loss function. We call this quantity the *gap negativity*. Since the negative sign problem becomes critical at lower temperatures, the gap negativity can be regarded as a temperature-independent quantity that characterizes its severity. Note that $\lambda(G)$ is independent of the choice of representation basis. Therefore, our aim now is to simply minimize the largest eigenvalue of G^+ .

B. Frustration-Free Systems

Although the formulation based on the negativity or the gap negativity is straightforward, the actual computational cost to evaluate Eq. (6) is exponentially high without further approximation or assumption. First, as a fundamental and natural requirement, we limit the unitary matrices for the basis transformation to those that can be expressed as a product of local unitary transformations. Mathematically, this requirement is expressed as

$$U = \otimes_i u_i, \quad (7)$$

where u_i is the local unitary transformation acting on the cell labeled by i . Theoretically, the cell can be chosen arbitrarily, and we can apply different unitary on each cell. However, in practice, we often select the cells as small repeating units, and the same local unitary transformation is shared across all cells. An example of the choice of cells is shown in Fig. 1.

To derive an approximation of the loss function, we additionally assume that the Hamiltonian under consideration possesses the frustration-free property [27–31]. While this assumption might appear overly restrictive at first glance, it is reasonable when considering the improvement of the negative sign problem through local basis transformations. Indeed, upon re-examining previous studies on analytical local transformation methods, it becomes apparent that the frustration-free property plays a crucial role in all spin models in which local basis transformation can eliminate the negative sign problem. Thus, for now, we will derive an approximation for the L1 adaptive loss under two assumptions: (1) local unitary transformations and (2) the frustration-free property.

The definition of frustration-free property is fairly simple:

Definition 1 (Frustration-free Hamiltonian). Consider a Hamiltonian written as $G = \sum_{b \in \mathcal{B}} g_b$, with e_b^0 being the ground state energy (or the largest eigenvalue) of g_b . If the ground state energy of the system is $\sum_{b \in \mathcal{B}} e_b^0$, then the Hamiltonian with this local Hamiltonian decomposition is called *frustration-free*.

Lemma 1 (Property of frustration-free Hamiltonian). If $G = \sum_{b \in \mathcal{B}} g_b$ is a frustration-free Hamiltonian, then its ground state (or the eigenstate associated with the largest eigenvalue) $|\psi_G\rangle$ is also the ground state of g_b , i.e., $g_b |\psi_G\rangle = e_b^0 |\psi_G\rangle$. Conversely, if there is a state $|\psi\rangle$ such that $g_b |\psi\rangle = e_b^0 |\psi\rangle$ for all b , G is a frustration-free Hamiltonian and $|\psi\rangle$ is the ground state of G . The proof of this lemma is given in Ref. 32.

It is important to note that frustration-free property is always defined with respect to the Hamiltonian G and its local Hamiltonian decomposition $G = \sum_{b \in \mathcal{B}} g_b$.

C. L1 Adaptive Loss

Although this may seem somewhat ad hoc, we define the L1 adaptive loss as follows:

Definition 2 (L1 adaptive loss). Let $G = \sum_{b \in \mathcal{B}} g_b$ be a Hamiltonian and u be a local unitary matrix acting uniformly on all sites. Then, the *L1 adaptive loss* is defined as

$$\begin{aligned} \mathcal{L}_{L1}(G, u) &= \frac{1}{|\mathcal{B}|} \sum_{b \in \mathcal{B}} \lambda^+((u \otimes u)g_b(u^\dagger \otimes u^\dagger)) - \lambda(g_b) \\ &= \max_{|\psi\rangle} \frac{1}{|\mathcal{B}|} \sum_{b \in \mathcal{B}} \sum_{i,j} \psi_i \psi_j^* |((u \otimes u)g_b(u^\dagger \otimes u^\dagger))_{ij}| \\ &\quad + \text{const}, \end{aligned} \quad (8)$$

where $|\mathcal{B}|$ is the number of bonds in the set of bonds \mathcal{B} and $|\psi\rangle$ is any normalized state of the system, i.e., $\sum_i |\psi_i|^2 = 1$. From the Perron-Frobenius theorem [33], as the eigenstate corresponding to the largest eigenvalue of A^+ can always be taken as a non-negative valued vector, we can assume that $|\psi\rangle_i$ is also non-negative without loss of generality. Embodying this, we can interpret Eq. (8) as a Min-Max optimization problem to minimize the L1 norm of the local Hamiltonian UgU^\dagger with each element weighted by $\psi_i \psi_j^*$. Since the vector $|\psi\rangle$ changes over time, we call this loss the *L1 adaptive loss*. Remember that $\lambda(A)$ is the largest eigenvalue of A and $\lambda^+(A)$ is defined as $\lambda(A^+)$, i.e., the largest eigenvalue of A^+ . Another important property of this loss function is that when the Hamiltonian has translational symmetry, this quantity can be defined independently of the system size. This property allows us to optimize local unitary transformation efficiently.

Remark 1. It is important to note that the stoquastic of G is not always expressed in the sum of stoquastic local Hamiltonians. This is because stoquastic operation involves taking absolute value element-wisely, which does not adhere to the distributive law. As a result, transforming the entire Hamiltonian into its stoquastic form is not equivalent to simply summing the stoquastic forms of its local components:

$$G^+ \neq \sum_{b \in \mathcal{B}} g_b^+. \quad (9)$$

Since the inconsistency between the left and right-hand sides in Eq. (10) is raised only at the overlapping sites of the local Hamiltonians, the difference between the two depends on the lattice connectivity, or more precisely, the ratio between area and volume of cells. This fact suggests that by taking large cells, the effect of the overlapping sites will be suppressed. It is important to note that in cases where the lattice connectivity is restricted to neighbors, we can still express G^+ as a sum of stoquastic local Hamiltonians. This is represented in the following equation:

$$G^+ = \sum_{n(b) \in \mathcal{B}} (\tilde{g}_{n(b)})^+. \quad (10)$$

Here, $n(b)$ denotes the set of all nearest neighbors involved in the bond b , and $\tilde{g}_{n(b)}$ is a local Hamiltonian that includes all the off-diagonal elements acting on b . In other words, it serves as a local Hamiltonian containing all the action supported on b . For the sake of simplicity, we will replace g_b with this local term in the following discussion. A detailed discussion of this remark can be found in the supplementary material of Ref. 12.

Although the L1 adaptive loss might appear to be insufficient in capturing the essence of the system, the following theorem guarantees that it provides a good approximation in the case of frustration-free quantum spin models.

Theorem 1. *The L1 adaptive loss gives the upper bound of gap negativity:*

$$\mathcal{L}_{L1}(G, u) \geq \lambda^+(G) - \lambda(G). \quad (11)$$

Proof. Since G^+ is a sum of local Hamiltonians g_b^+ , we have

$$\lambda^+(G) \leq \sum_{b \in \mathcal{B}} \lambda^+(g_b). \quad (12)$$

Then, since the Hamiltonian is frustration-free, the following inequality is derived:

$$\sum_b \lambda(g_b) - \lambda^+(g_b) \geq \lambda(G) - \lambda^+(G) \geq 0. \quad (13)$$

By using Definition 2, we can prove Theorem 1. \square

In deriving the L1 adaptive loss, we initially assumed the frustration-free property. However, even in cases where the Hamiltonian is not strictly frustration-free, this quantity is expected to serve as a good approximation of the average sign, particularly when the system's ground state closely resembles that of the local Hamiltonians. In other words, the L1 adaptive loss remains a good approximation when the original Hamiltonian has a certain frustration-freeness [34]. Furthermore, by recognizing that all previously studied loss functions can be expressed as $\sum_{ij} |(u \otimes u)g_b(u^\dagger \otimes u^\dagger)|_{ij}$, which is essentially the L1 loss of the local Hamiltonians, we can identify a key distinction: Previous loss functions assumed that the ground state is a uniform wave function in the transformed basis, whereas the L1 adaptive loss recalculates the ground state at each iteration, hence, providing a more accurate approximation.

V. NUMERICAL RESULT

Based on the above discussion, we will demonstrate through numerical optimization that the negative sign problem can indeed be mitigated. Before actually examining the research results, let us briefly explain the environmental settings and approaches used in the numerical calculations. It should be noted that our optimization method is independent of the specific choice of Markov chain Monte Carlo (MCMC) [35–37] sampling algorithm employed. In our case, we used the modified worm algorithm to simulate local degrees of freedom beyond binary values by accommodating general integer degrees of freedom. The transition kernel of the worm algorithm is designed to minimize the rejection rate during the worm updating process as explained in Ref. 38. Additionally, our generalized worm algorithm incorporates warp updates to introduce single-site updates [39]. Regarding the optimization method using local basis transformations, we employed the Riemannian gradient descent algorithm [40–43] and used Adam as the optimizer [44].

This section is structured as follows: First, we demonstrate a proof of concept by applying our optimization method to artificially constructed one-dimensional (1D) and two-dimensional (2D) frustration-free models. Following this, we present the results of our method for models studied in previous analytical research, which use local basis transformations based on physical intuition to eliminate the negative sign problem, including the J_0 - J_1 - J_2 - J_3 model, bilinear-biquadratic chain, frustrated ladder, and Shastry-Sutherland model. Finally, we show that it is also possible to mitigate the negative sign problem to some extent in the kagome Heisenberg model, which has strong frustrations.

A. Randomly Generated Frustration-Free Model

As the derivation of the L1 adaptive loss function, Eq. (8), highly depends on the frustration-free property of the Hamiltonian, we demonstrate the applicability of our optimization scheme to randomly generated Hamiltonians belonging to this class.

First, we consider frustration-free models defined on a chain lattice. For simplicity, only the model Hamiltonians with translational invariance and periodic boundary conditions (PBC) will be our primal test cases. To generate 1D frustration-free models, we exploit the concept of the parent Hamiltonian [45, 46] that can be defined as a matrix product state (MPS) [47]. In the present simulation, we construct frustration-free models as a parent Hamiltonian of random matrix product state with bond dimension $\chi = 2$ defined on chain lattice with three-dimensional local Hilbert space. By construction, the local Hamiltonian is a projection matrix. Thus, the loss function can always be in the range $[0, 1]$. As a benchmark, first, we perform our algorithm on 1,000 random 1D frustration-free models and plot the histogram of the gap negativity before and after optimization in Fig. 2. One can see that the red histogram (optimized) is more concentrated and distributed in lower negativity regions, while the blue histogram (original) is more spread out. This outcome effectively demonstrates the performance of our algorithm in systematically reducing the negativity in 1D randomly generated frustration-free models.

Next, Fig. 3 shows the relation between the negativity and the L1 adaptive loss function. The figure illustrates the change in the negativity and the L1 adaptive loss function before and after the optimization. The data points in the upper right corner indicate a significant reduction in the L1 adaptive loss function compared to its pre-optimization value and a substantial alleviation of the negative sign in the system Hamiltonian. A notable characteristic of this plot is the linear correlation observed across the data, suggesting that negativity acts as a decreasing function of the L1 adaptive loss function. This linear relationship is indeed a consequence of Theorem 1, in this specific instance with $L = 6$. In the plot, there is a black line representing $y = 6x$. The coefficient

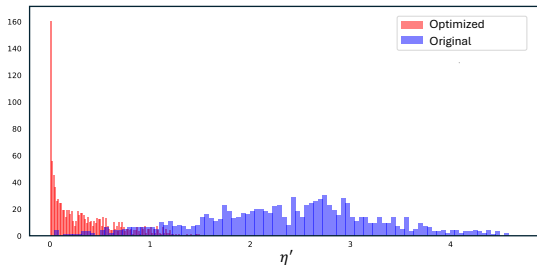


FIG. 2. Histogram of gap negativity η' before and after the optimization for 1D random frustration-free models with $L = 6$. The blue histogram represents the gap negativity of the original Hamiltonian, and the red histogram represents the gap negativity of the optimized Hamiltonian. Optimization is done by minimizing the L1 adaptive loss function for cell type (a) in Fig. 1. Evaluation of the gap negativity is done by exact diagonalization of the system Hamiltonian and its stoquastic.

6 comes from the fact $|\mathcal{B}| = 6$. One can observe most of the points are indeed below this line, while there are some points exceeding this line. This happens due to the fact that the local Hamiltonian we optimized here is not \tilde{g}^+ [Eq. (9)]. However, this extra negativity will be less influential in cell type (b) in Fig. 1, where the unitary transformation is applied to two sites. One can indeed confirm this by noting that red points are more concentrated below the black line. This is because the effect of the sign problem existing at the edges of the cells contributes less to the entire negativity in cell type (b). See the discussion in Remark 1.

We also demonstrate the effectiveness of our method for 2D frustration-free models. We generate 1,000 Projected Entangled Pair States (PEPS) [48] and construct their parent Hamiltonians based on the idea explained in Refs. 49 and 50. In constructing the parent Hamiltonians, it is necessary to set the bond dimension to at least 8 (it is three in the 1D case). Consequently, our 2D frustration-free models defined on a square lattice have a local Hilbert space with dimension 8. A histogram illustrating the extent to which our optimization method has mitigated the negative sign compared to the original 2D frustration-free Hamiltonians is presented in Fig. 4. As observed in the figure, the gap negativity η' after the optimization is significantly reduced compared to η' for the original Hamiltonians. Note $\eta' = 0$ means that the negative sign is removed completely. This reduction of the gap negativity indicates improvement in the negative sign by our method, demonstrating its effectiveness in addressing the negative sign problem of 2D quantum spin systems as well. Considering that previous studies on the negative sign problem have scarcely reported results on mitigating in 2D models, the present outcome has significant importance. Indeed, the only previously known result about reducing the sign problem for the 2D case is Ref. 19, and thus, the present result is a major advance in that it provides a robust methodology for addressing

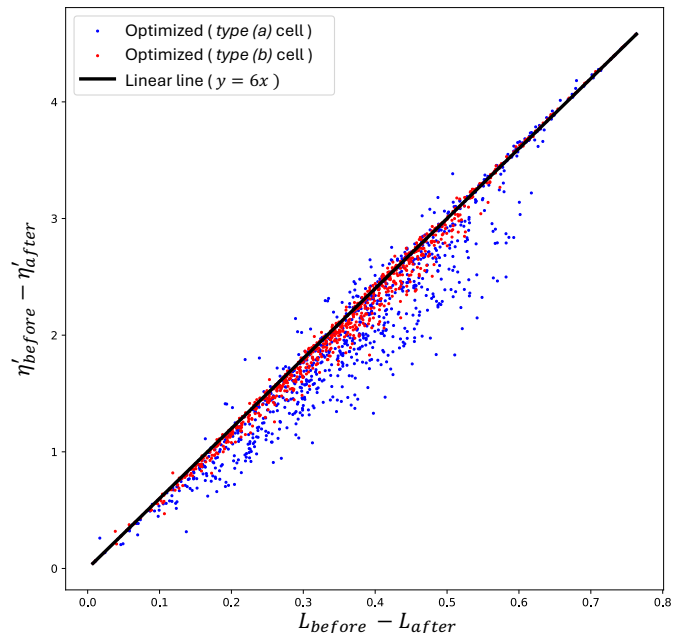


FIG. 3. Scatter plot of improvements in gap negativity (vertical axis) and L1 adaptive loss function (horizontal axis) for 1D random frustration-free models with $L = 6$. The improvement of gap negativity and loss function is defined as $\eta'_{\text{before}} - \eta'_{\text{after}}$ and $\mathcal{L}_{\text{before}} - \mathcal{L}_{\text{after}}$, respectively. Blue dots show the results using cell type (a) in Fig. 1 and red dots with cell type (b).

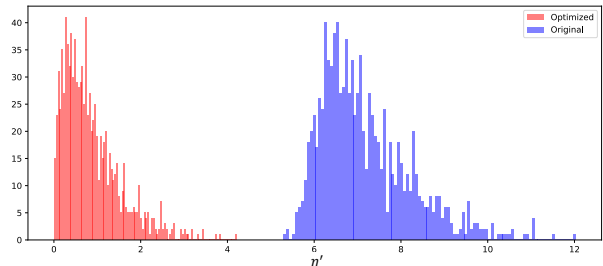


FIG. 4. Histogram of gap negativity η' for original Hamiltonian (blue) and for optimized Hamiltonian (red) for 2D random frustration-free models.

this complex challenge in quantum simulation.

B. Benchmark on Models with Known Negative-Sign-Free Transformations

There are several frustration-free models for which local basis transformations that eliminate the negative sign are known analytically. As described in Section IV B, our proposed loss function is inspired by the frustration-free property. This background on the design of the loss function suggests that optimizing the L1 adaptive loss func-

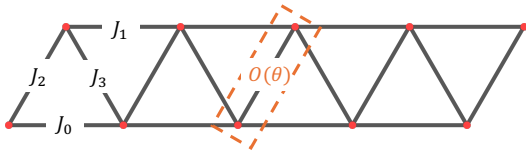


FIG. 5. Lattice structure and cell for basis transformation for the J_0 - J_1 - J_2 - J_3 model. We only consider the case when $J_0 = J_1 = 1$.

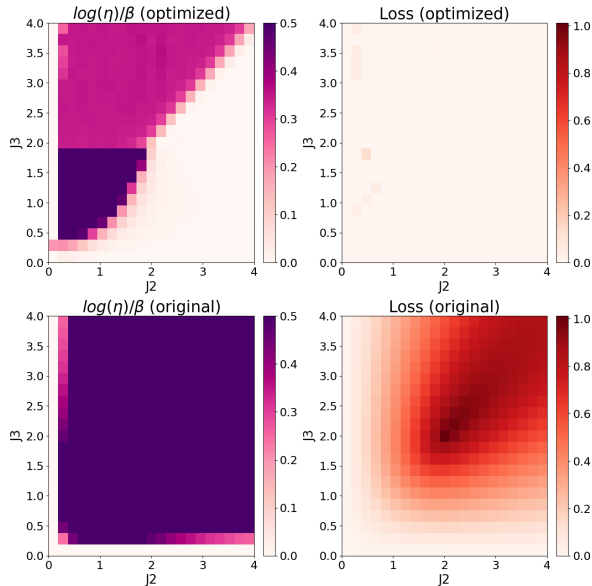


FIG. 6. Gap negativity $\eta' \approx \log(\eta)/\beta$ (left) and L1 adaptive loss function (right) before (bottom) and after (top) the optimization for the J_0 - J_1 - J_2 - J_3 model at $\beta = 4$. The next nearest neighbor interactions J_0 and J_1 are fixed to unity, and the heat map is plotted for various J_2 and J_3 . Simulation is done for $L = 10$. Color gradients indicate the magnitude of $\log(\eta)/\beta$ or the L1 adaptive loss function: The lighter the color, the better.

tion should be able to reconstruct the analytically derived local basis transformations or other optimal transformations similar to it. In this section, we rigorously examine this postulation by applying our methodology to various quantum spin models and compare with established theoretical predictions.

1. J_0 - J_1 - J_2 - J_3 Model

First, we apply our method to the J_0 - J_1 - J_2 - J_3 model, which is a spin-1/2 Heisenberg chain with nearest-neighbor antiferromagnetic interactions J_2 and J_3 and next-nearest-neighbor antiferromagnetic interactions J_0 and J_1 . We choose the cells for local orthogonal basis transformation as shown in Fig. 5. In the simulation, J_0 and J_1 are fixed to unity. The result is shown in Fig. 6. In Ref. 17, the authors analytically found that the negative sign can be completely removed when

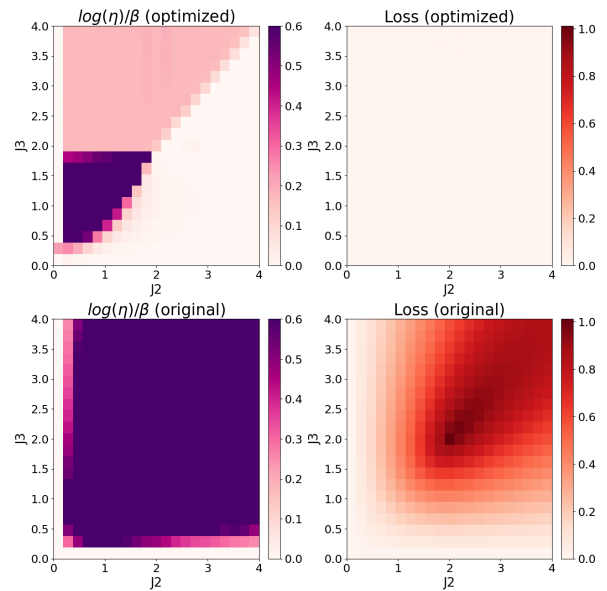


FIG. 7. Gap negativity $\eta' \approx \log(\eta)/\beta$ (left) and L1 adaptive loss function (right) before (bottom) and after (top) the optimization for the J_0 - J_1 - J_2 - J_3 model at $\beta = 8$.

$J_3 > J_1 + J_0 = 2$ with dimer-like basis rotation. In Fig. 6, the negative sign is mitigated for $J_3 < J_2$, while the region $J_3 > 2 \cap J_3 > J_2$ still appears to be affected by the negative sign. The reason for the apparent persistence of the negative sign in this region is that, although $\log(\eta)/\beta$ reaches the minimum value after optimization, the degeneracy of the ground state increases compared to the original Hamiltonian G . The reason for the apparent persistence of the negative sign in this region is that, although $\log(\eta)/\beta$ reaches the minimum value after optimization, the degeneracy of the ground state increases compared to the original Hamiltonian G . However, since this degeneracy only affects the negative sign by a constant factor, the average sign does not diverge at low temperatures. This implies that we are not fundamentally facing the negative sign problem in this region. This can also be seen from Figs. 6 and 7, where $\log(\eta)/\beta$ approaches zero as the temperature decreases. Thus, we conclude that the negative sign problem has been resolved for $J_3 > 2 \cup J_3 < J_2$, which includes the results in Ref. 17.

2. Bilinear-Biquadratic Chain

Next, we consider the $S = 1$ bilinear-biquadratic (BLBQ) chain model. The Hamiltonian encapsulates a range of significant models, with the parameter α tuning the system through various quantum states from the nearest-neighbor antiferromagnetic Heisenberg chain ($\alpha = 0$) to the AKLT model ($\alpha = 1/3$) and even to the intriguing SU(3) chain, which can be solved exactly by the Bethe ansatz [51], at $\alpha = 1$. The Hamiltonian of the

$S = 1$ BLBQ chain is defined as

$$G = \sum_i g_{i,i+1}, \quad (14)$$

where the local interaction term $g_{i,i+1}$ is given by

$$g_{i,i+1} = -\mathbf{S}_i \cdot \mathbf{S}_{i+1} - \alpha[(\mathbf{S}_i \cdot \mathbf{S}_{i+1})^2 - 1]. \quad (15)$$

Here, \mathbf{S} represents the $S = 1$ spin operator.

In our simulation, we employ cell type (a) in Fig. 1. Building upon the original definition of the BLBQ model, we also examine the case where a finite transverse magnetic field h_x is applied. Typically, the transverse magnetic field is known to induce negative signs. Since we know from the previous work that local unitary transformation can remove the negative sign, we can expect our method to also work well at the AKLT point and surrounding region ($\alpha < 1$). The heat map of the negativity and loss function before and after the optimization is depicted in Fig. 8. First, as analytically predicted, the negative sign is completely removed for $\alpha < 1$, as illustrated in the $h_x = 0$ section of Fig. 8. While this result aligns perfectly with expectations, it does come as a bit of a surprise to us. The reason is that the local basis transformation theoretically identified in Ref. 20 is a unitary matrix, including complex elements, whereas, in the present study, we explore orthogonal matrices only. Furthermore, we empirically confirm that our algorithm can get rid of the negative signs due to the transverse magnetic field, which can also be seen in regions $\alpha < 1$ with $h_x > 0$ in Fig. 8. This finding demonstrates that our method can be applied to a broader range of models than just the frustration-free system.

3. Shastry-Sutherland Model

As a final example of the frustration-free models, we examine the Shastry-Sutherland model, a 2D frustrated spin model with known negative-sign-free local basis transformation [19, 24]. The lattice structure and the cell for the local basis transformation are shown in Fig. 9. This model exhibits a wide variety of quantum phases, including dimer-singlet, spin liquid, Néel order, and plaquette-singlet [52, 53], making it one of the most important examples in 2D frustrated systems. It is known that, in the parameter region where J_1/J_d and J_2/J_d are small, the system becomes frustration-free, and the ground state is a unique dimer-singlet product state. We choose the cells for the local basis transformation as shown in Fig. 9. As seen in Fig. 10, for the parameter region with smaller J_1/J_d and J_2/J_d , we observe the negativity is completely removed. This is an expected result as the system becomes frustration-free around this parameter region. Also, we confirm that the parameter of $J_1 = J_2$ does not suffer from the negative sign problem with the analytical dimer basis as well as with our optimized basis. The only apparent difference between the

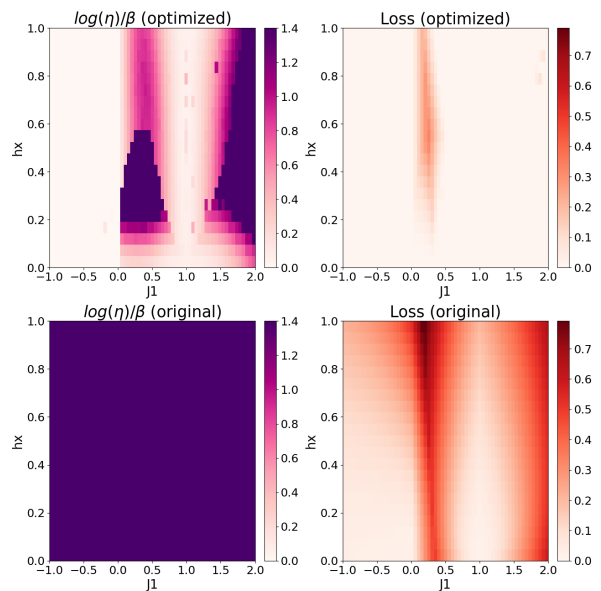


FIG. 8. Gap negativity $\eta' \approx \log(\eta)/\beta$ (left) and L1 adaptive loss function (right) before (bottom) and after (top) the optimization for the BLBQ model at $\beta = 4$. Simulation is done for $L = 10$ with open boundary conditions. Color gradients indicate the magnitude of $\log(\eta)/\beta$ or the L1 adaptive loss function: The lighter the color, the better.

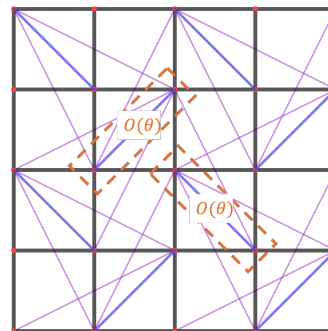


FIG. 9. Shastry-Sutherland model defined on the 2D square lattice. The black, pink, and blue edges denote the Heisenberg interaction with coupling constant J_d , J_1 , and J_2 , respectively. The cells for two-site basis transformation are denoted by dashed orange rectangles.

analytical solution (dimer basis) and our optimized basis is that the region deviated from the diagonal line $J_1 = J_2$. In the dimer basis, the negativity remains small in a wide region around $J_1 = J_2$. In our optimized basis, however, the negativity becomes unity only when $J_1 = J_2$.

The observed difference between the dimer-product basis and the optimized basis can be attributed to the nature of our loss function, which is not guaranteed to approximate the average sign when the system is not frustration-free. Conversely, this result can also be interpreted as evidence that even a small deviation from the diagonal line $J_1 = J_2$ causes the Shastry-Sutherland model to deviate significantly from the frustration-free

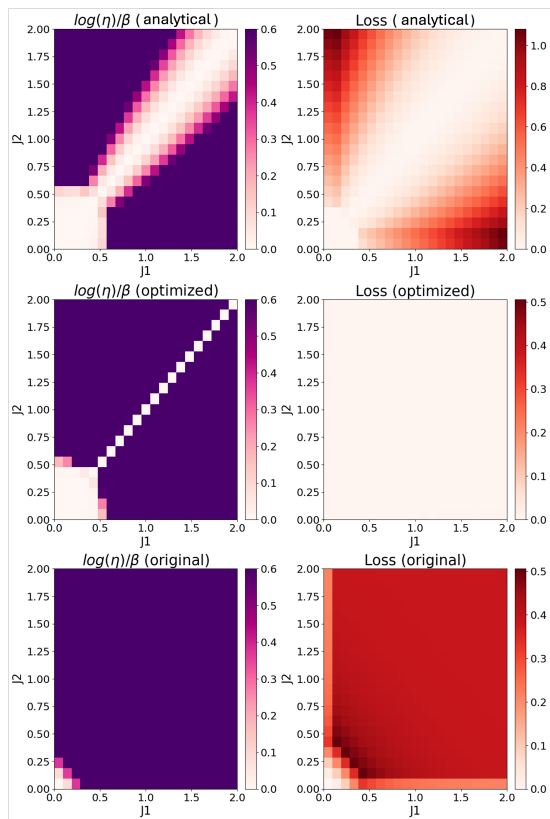


FIG. 10. Gap negativity $\eta' \approx \log(\eta)/\beta$ (left) and L1 adaptive loss function (right) before (bottom) and after (middle) the optimization for the Shastry-Sutherland model at $\beta = 4$ with $N = 4 \times 4$. For comparison, the results using the dimer-product basis are also presented in the top row.

property. Nevertheless, it is important to note that the analytically derived basis also suffers from the sign problem at low temperatures in the parameter region slightly off the diagonal line, as shown in Fig. 11. This means that both the analytically derived basis and our optimized basis behave similarly at low temperatures.

C. Kagome Heisenberg Model

Lastly, we apply our method to the Heisenberg model on the kagome lattice as a promising candidate to exhibit exotic quantum-dynamical behavior such as spin liquid [54]. The precise nature of its ground state, as well as finite temperature properties, however, remains actively debated, with proposed possibilities including valence bond crystals ground states [55]. From a computational perspective, the kagome Heisenberg model poses significant difficulties due to frustrating interactions and its intrinsic 2D structure. While some techniques like exact diagonalization are limited to small system sizes, and density matrix renormalization group studies have relied on the quasi-1D approximation of cylinders or strips, QMC stands out in its potential ability to simulate large

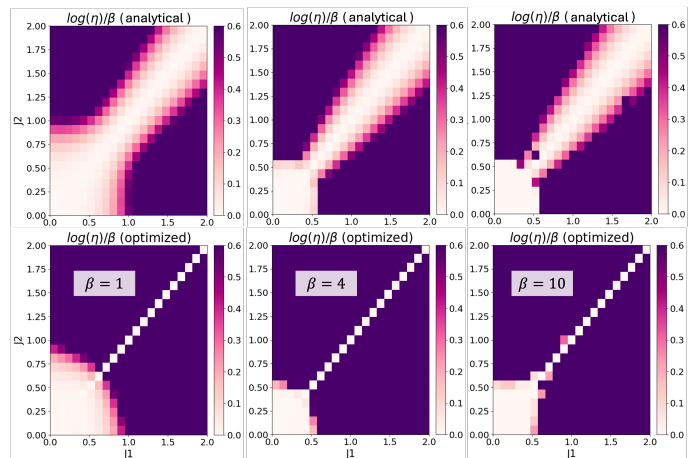


FIG. 11. Gap negativity $\eta' \approx \log(\eta)/\beta$, of the Shastry-Sutherland model at different temperatures. The first row is the result using the dimer-product basis, and the second row is the result using the optimized basis. Note that even for the analytically derived basis, the parameter region, except for the diagonal line and the bottom-left square exhibits the severe negative sign problem at low temperatures. For example, $\log(\eta)/\beta = 0.345$ at $J_1 = 0.8$, $J_2 = 1.0$, and this is about $\eta^{-1} = \langle S \rangle = 0.0317$ at $\beta = 10$, which requires around 1,000 times more Monte Carlo steps to achieve the same accuracy as the one without negative sign problem.

2D kagome lattices. Unfortunately, the presence of frustrating antiferromagnetic interactions makes the QMC simulation of the kagome Heisenberg model a challenging task [56].

There is previous research on alleviating the negative sign problem for the kagome Heisenberg model. In Ref. 57, we confirmed that with a strong transverse magnetic field ($h_x/J \sim 4$), the negative sign disappears at low temperatures, without any basis transformation. This can be understood from the fact that for any model, the negative sign vanishes in limits where the transverse field becomes dominant. While an interesting result, especially showing the phenomenon of the sign disappearing only at low temperatures, as seen in the Shastry-Sutherland model, this approach has greatly limited applicability. In the present numerical experiments, there is no transverse magnetic field, or only a weak field is applied. The cell is taken to contain three sites as shown in Fig. 12. We analyze the cases where the interaction is anisotropic: J_z is fixed to unity, while J_x and J_y are changed from -2 to 2. We confirm that the negative sign is alleviated in certain parameter region Fig. 11. These results also lead to an intriguing conjecture: our method almost entirely eliminates the negative sign caused by the transverse magnetic field. In fact, by comparing (a) and (c) with (b) and (d) in Fig. 11, we can see that the effect of the magnetic field on the negative sign is removed to a large extent. Another noteworthy observation is that, without a transverse magnetic field, the model is invariant under the exchange between J_x and J_y . However, in

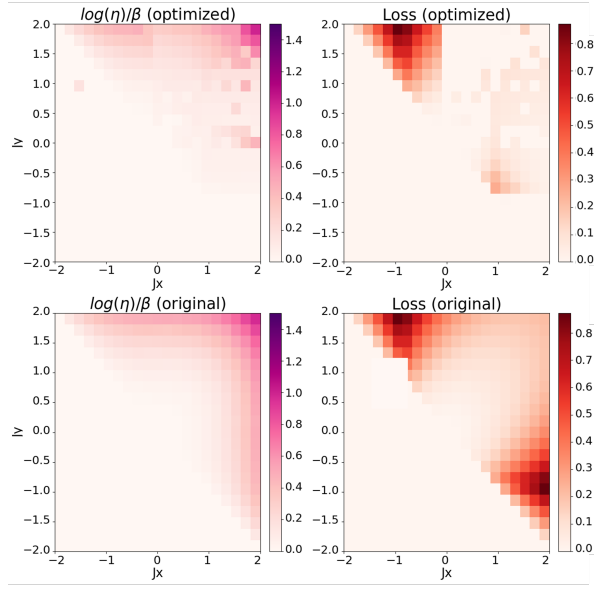
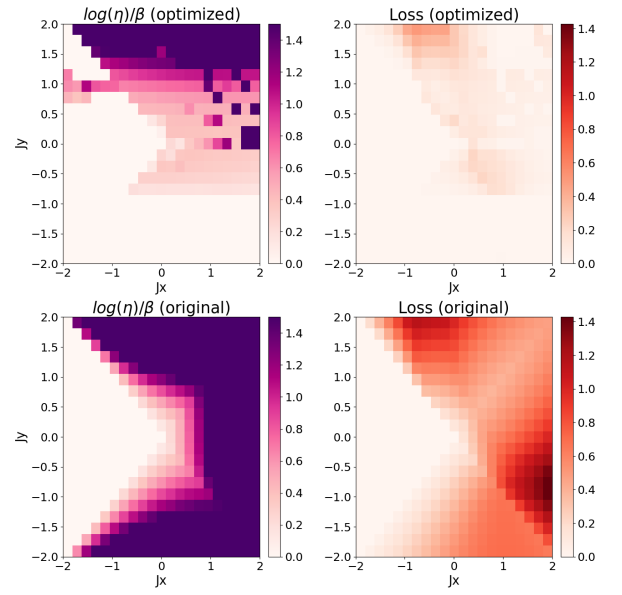
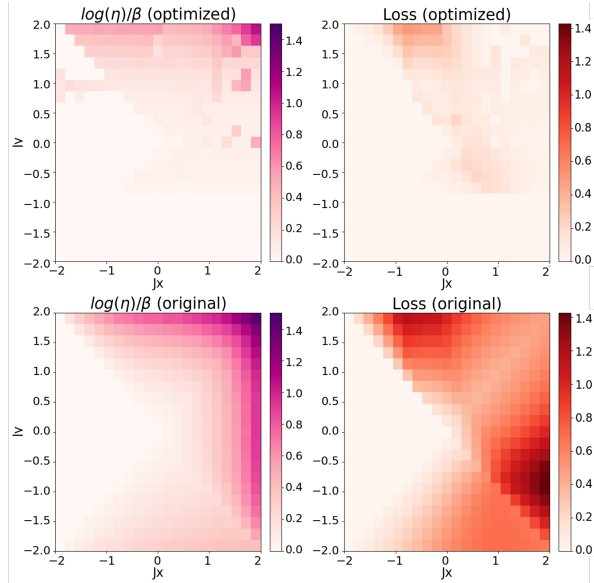
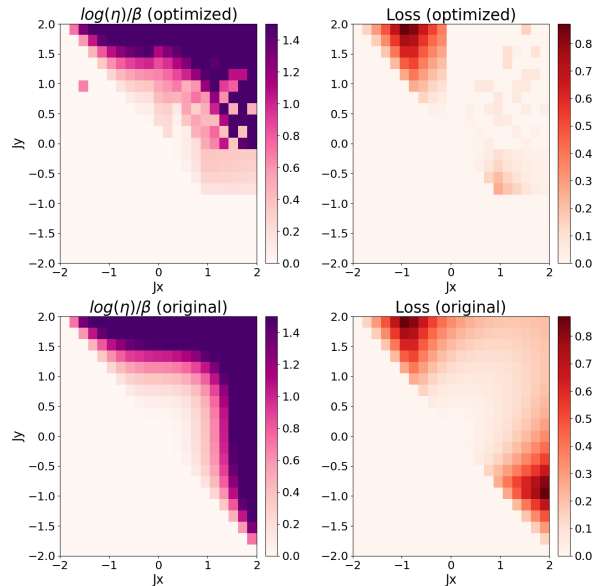
(a) Simulation at $\beta = 0.25, h_x = 0$ (d) Simulation at $\beta = 0.5, h_x = 0.5$ (b) Simulation of $\beta = 0.25, h_x = 0.5$ (c) Simulation at $\beta = 0.5, h_x = 0$

FIG. 11. Gap negativity $\eta' \approx \log(\eta)/\beta$ (left) and L1 adaptive loss function (right) before (bottom) and after (top) the optimization for the anisotropic kagome Heisenberg model at $(\beta, h_x) = (0.25, 0)$ (a), $(0.25, 0.5)$ (b), $(0.5, 0)$ (c), and $(0.5, 0.5)$ (d). The coupling constant J_z is fixed to 1, with the vertical axis representing J_y and the horizontal axis representing J_x , both ranging from -2 to 2. Each heatmap should be interpreted in the same way as in the other figures. The system size is $N = 5 \times 5$. We confirmed that $N = 4 \times 4$ and 6×6 system sizes give similar results.

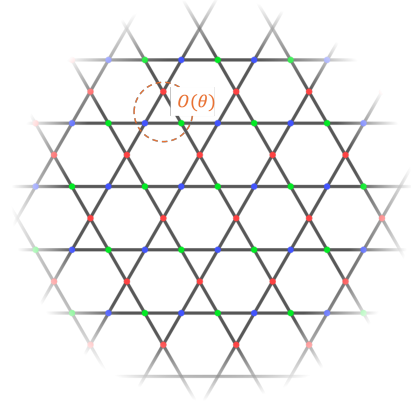


FIG. 12. Lattice structure of the kagome Heisenberg model and cell for three-site basis transformation. In the figure, we combine the three sites into a single cell.

our results, this symmetry is broken, as seen clearly in Fig. 11. This issue, which is explored in more detail in the next section, arises because we permit only orthogonal transformations as the local basis transformations.

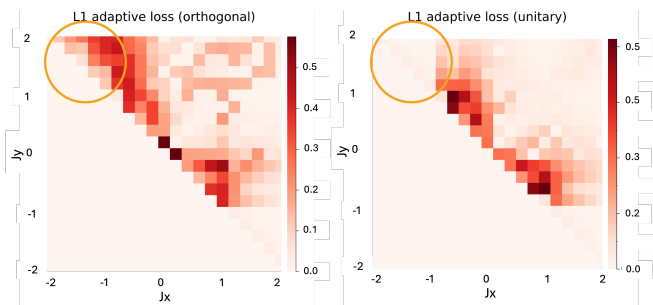


FIG. 13. Comparison of L1 adaptive loss function with unitary and orthogonal transformations after optimization for the kagome Heisenberg Model at $J_z = 1$ and $h_x = 0$. The left figure is the result of the orthogonal transformation, and the right figure is the result of the unitary transformation. Orange circle indicate the region where the negativity is removed only by the unitary transformation.

VI. ORTHOGONAL VS UNITARY TRANSFORMATIONS

The numerical experiments in the previous sections as well as in previous studies [12, 15, 21], only orthogonal transformations were considered as local transformations. However, it is worth noting that in QMC, the weights can be complex values, which allows for the use of unitary transformations. Here, we explore the possibility that utilizing unitary transformations could further mitigate the negative sign problem. We demonstrate it by comparing the results of unitary and orthogonal transformations applied to the kagome Heisenberg Model. As seen in Fig. 11 in Section V C, if we optimize within orthogonal transformations, the inherent symmetry under the exchange of J_x and J_y was broken. However, when allowing for transformations that include unitary transformations, the symmetry is restored as shown in Fig. 13. This is a highly intriguing result, indicating that even though the original Hamiltonian is a real symmetric matrix, using unitary matrices instead of orthogonal ones can break the real symmetry to potentially mitigate the negative sign problem even more.

VII. CONCLUSION

In the present study, we first introduced a unified metric specifically designed to represent the severity of the

negative sign problem. This metric not only facilitates a cohesive treatment of both reweighting and basis transformation methods, but it also serves as a definitive indicator of the severity of the negative sign. All other metrics employed to address the negative sign problem in the future should ideally be derived from this foundational measure, ensuring a consistent and comprehensive approach to quantifying and mitigating the issue. A key finding from our investigation was the realization that employing the stoquastic form of Hamiltonian G^+ as a virtual Hamiltonian G_v in reweighting is always the optimal selection in terms of negativity.

Particularly, we formulated the basis transformation methods as an optimization problem, and focused mainly on the L1 adaptive loss function we devised under the assumption of the frustration-free property. This property is a commonly observed characteristic in quantum spin models where local basis transformation methods are analytically known to function effectively. We then applied this optimized approach to several quantum spin models. Our method demonstrated excellent performance, single-handedly reproducing almost all previously discovered basis transformations found in various studies. The implications of this research are substantial, offering a new lens through which the negative sign problem can be approached and potentially mitigated, even in quantum spin systems where analytical solutions are unknown.

However, the study also revealed certain limitations. Although our method performed more than expected in some models with no relation to the frustration-free property, the method does not guarantee the improvement of the negative sign problem and shows potential inaccuracies when applied outside the frustration-free domain. Additionally, we found that the method exhibited lower improvement rates in 2D systems compared to its great success in 1D systems. These limitations likely stem from the approximate nature of the L1 adaptive loss function, which may not fully encapsulate the complexities of lattice structures.

ACKNOWLEDGMENTS

The authors would like to thank Tsuyoshi Okubo and Hidemaro Suwa for discussions and comments. This work was supported by the Center of Innovation for Sustainable Quantum AI, JST Grant Number JPMJPF2221, JSPS KAKENHI Grant Numbers JP20H01824 and JP24K00543, and JSPS KAKENHI Grants No. JP24KJ0892.

[1] M. Suzuki, editor. *Quantum Monte Carlo Methods in Condensed Matter Physics*. World Scientific, Singapore, 1994.

[2] Adolfo Avella and Ferdinando Mancini, editors. *Strongly*

Correlated Systems: Numerical Methods, volume 176 of *Springer Series in Solid-State Sciences*. Springer, Berlin, Heidelberg, 2013.

[3] J. Gubernatis, N. Kawashima, and P. Werner. *Quan-*

- tum Monte Carlo Methods: Algorithms for Lattice Models*. Cambridge University Press, 2016.
- [4] Hans Gerd Evertz, Gideon Lana, and Mihai Marcu. Cluster algorithm for vertex models. *Phys. Rev. Lett.*, 70(7):875–879, February 1993.
- [5] Syngae Todo. Loop Algorithm. In Adolfo Avella and Ferdinando Mancini, editors, *Strongly Correlated Systems: Numerical Methods*, pages 153–184. Springer, Berlin, Heidelberg, 2013.
- [6] N. V. Prokof'ev, B. V. Svistunov, and I. S. Tupitsyn. Exact, complete, and universal continuous-time world-line Monte Carlo approach to the statistics of discrete quantum systems. *Soviet Physics JETP*, 87:310, 1998.
- [7] O. F. Syljuasen and A. W. Sandvik. Quantum Monte Carlo with directed loops. *Phys. Rev. E*, 66:046701, 2002.
- [8] A W Sandvik and J Kurkijärvi. Quantum Monte Carlo simulation method for spin systems. *Phys. Rev. B*, 43(7):5950–5961, March 1991.
- [9] Tota Nakamura, Naomichi Hatano, and Hidetoshi Nishimori. Reweighting method for quantum Monte Carlo simulations with the negative-sign problem. *J. Phys. Soc. Jpn.*, 61(10):3494–3502, October 1992.
- [10] Naomichi Hatano. Data analysis for quantum Monte Carlo simulations with the negative-sign problem. *J. Phys. Soc. Jpn.*, 63(5):1691–1697, May 1994.
- [11] Tota Nakamura. Vanishing of the negative-sign problem of quantum monte carlo simulations in one-dimensional frustrated spin systems. *Phys. Rev. B*, 57(6):R3197–R3200, February 1998.
- [12] Dominik Hangleiter, Ingo Roth, Daniel Nagaž, and Jens Eisert. Easing the Monte Carlo sign problem. *Sci. Adv.*, 6(33):eabb8341, 2020.
- [13] Hakop Pashayan, Joel J. Wallman, and Stephen D. Bartlett. Estimating outcome probabilities of quantum circuits using quasiprobabilities. *Phys. Rev. Lett.*, 115(7):070501, 2015.
- [14] Naomichi Hatano and Masuo Suzuki. Representation basis in quantum Monte Carlo calculations and the negative-sign problem. *Phys. Lett. A*, 163(4):246–249, 1992.
- [15] Ryan Levy and Bryan K. Clark. Mitigating the sign problem through basis rotations. *Phys. Rev. Lett.*, 126(21):216401, 2021.
- [16] Tota Nakamura, Satoshi Takada, Kiyomi Okamoto, and Naoki Kurosawa. Haldane and dimer gap in general double spin-chain models. *J. Phys.: Condens. Matter*, 9(30):6401, jul 1997.
- [17] Tota Nakamura. Vanishing of the negative-sign problem of quantum Monte carlo simulations in one-dimensional frustrated spin systems, July 1997.
- [18] Stefan Wessel, B. Normand, Frédéric Mila, and Andreas Honecker. Efficient quantum Monte Carlo simulations of highly frustrated magnets: The frustrated spin-1/2 ladder. *SciPost Phys.*, 3:005, 2017.
- [19] Stefan Wessel, Ido Niesen, Jonas Stapmanns, B. Normand, Frédéric Mila, Philippe Corboz, and Andreas Honecker. Thermodynamic properties of the Shastry-Sutherland model from quantum Monte Carlo simulations. *Phys. Rev. B*, 98:174432, 2018.
- [20] Kouichi Okunishi and Kenji Harada. Symmetry-protected topological order and negative-sign problem for $SO(N)$ bilinear-biquadratic chains. *Phys. Rev. B*, 89:134422, 2014.
- [21] Milad Marvian, Daniel A Lidar, and Itay Hen. On the computational complexity of curing non-stoquastic Hamiltonians. *Nat. Commun.*, 10(1):1571, April 2019.
- [22] Joel Klassen, Milad Marvian, Stephen Piddock, Marios Ioannou, Itay Hen, and Barbara M Terhal. Hardness and ease of curing the sign problem for two-local qubit Hamiltonians. *SIAM J. Comput.*, 49(6):1332–1362, January 2020.
- [23] Fabien Alet, Kedar Damle, and Sumiran Pujari. Sign-problem-free Monte Carlo simulation of certain frustrated quantum magnets. *Phys. Rev. Lett.*, 117:197203, 2016.
- [24] Shin Miyahara and Kazuo Ueda. Exact dimer ground state of the two dimensional heisenberg spin system $SrCu_2(BO_3)_2$. *Phys. Rev. Lett.*, 82(18):3701–3704, 1999.
- [25] Hidehiko Kohshiro, Ryui Kaneko, Satoshi Morita, Hoshio Katsura, and Naoki Kawashima. Multiple magnetization plateaus induced by farther neighbor interaction in an $S = 1$ two-leg Heisenberg spin ladder, February 2021.
- [26] A. Honecker, S. Wessel, R. Kerkdyk, T. Pruschke, F. Mila, and B. Normand. Thermodynamic properties of highly frustrated quantum spin ladders: Influence of many-particle bound states. *Phys. Rev. B*, 93(5):054408, February 2016.
- [27] Walter Selke. The ANNNI model — theoretical analysis and experimental application. *Phys. Rep.*, 170(4):213–264, November 1988.
- [28] I Peschel and V J Emery. Calculation of spin correlations in two-dimensional Ising systems from one-dimensional kinetic models. *Z. Phys. B: Condens. Matter*, 43(3):241–249, September 1981.
- [29] A. Yu Kitaev. Fault-tolerant quantum computation by anyons, 2003.
- [30] D S Rokhsar and S A Kivelson. Superconductivity and the quantum hard-core dimer gas. *Phys. Rev. Lett.*, 61(20):2376–2379, November 1988.
- [31] Ian Affleck, Tom Kennedy, and Hal Lieb, Elliott Gand Tasaki. Valence bond ground states in isotropic quantum antiferromagnets. *Commun. Math. Phys.*, 115(3):477–528, September 1988.
- [32] Hal Tasaki. *Physics and Mathematics of Quantum Many-Body Systems*. Springer, 2020.
- [33] Oskar Perron. Zur theorie der matrices. *Math. Ann.*, 64(2):248–263, June 1907.
- [34] Jun Takahashi, Chaithanya Rayudu, Cunlu Zhou, Robbie King, Kevin Thompson, and Ojas Parekh. An $SU(2)$ -symmetric semidefinite programming hierarchy for quantum max cut, 2023.
- [35] Christian Robert and George Casella. *Monte Carlo Statistical Methods*. Springer texts in statistics. Springer, New York, NY, November 2010.
- [36] David P Landau and Kurt Binder. *A guide to Monte Carlo simulations in statistical physics*. Cambridge University Press, Cambridge, England, 4 edition, November 2014.
- [37] M E J Newman and G T Barkema. *Monte Carlo Methods in Statistical Physics*. Oxford University Press, 02 1999.
- [38] Hidemaro Suwa and Syngae Todo. *Geometric Allocation Approach for the Transition Kernel of a Markov Chain*, pages 213–222. De Gruyter, Berlin, Boston, 2013.
- [39] Hidemaro Suwa. *Geometrically Constructed Markov Chain Monte Carlo Study of Quantum Spin-Phonon Complex Systems*. Springer Japan, 2012.
- [40] Traian E Abrudan, Jan Eriksson, and Visa Koivunen. Steepest descent algorithms for optimization under uni-

- tary matrix constraint. *IEEE Trans. Signal Process.*, 56(3):1134–1147, April 2008.
- [41] Traian Abrudan, Jan Eriksson, and Visa Koivunen. Conjugate gradient algorithm for optimization under unitary matrix constraint. *Signal Processing*, 89(9):1704–1714, September 2009.
- [42] Mario Lezcano-Casado. Trivializations for gradient-based optimization on manifolds. In *Advances in Neural Information Processing Systems (NeurIPS)*, pages 9154–9164, 2019.
- [43] Mario Lezcano-Casado and David Martínez-Rubio. Cheap orthogonal constraints in neural networks: A simple parametrization of the orthogonal and unitary group. In *International Conference on Machine Learning (ICML)*, pages 3794–3803, 2019.
- [44] Diederik P Kingma and Jimmy Ba. Adam: A method for stochastic optimization, December 2014.
- [45] D. Perez-Garcia, F. Verstraete, M. M. Wolf, and J. I. Cirac. Matrix product state representations. *Quantum Inf. Comput.*, 7:401–430, 2007.
- [46] Carlos Fernández-González, Norbert Schuch, Michael M Wolf, J Ignacio Cirac, and David Pérez-García. Frustration free gapless Hamiltonians for matrix product states. *Commun. Math. Phys.*, 333:299–333, 2015.
- [47] A Klümper, A Schadschneider, and J Zittartz. Matrix product ground states for one-dimensional spin-1 quantum antiferromagnets. *EPL*, 24(4):293–297, November 1993.
- [48] Román Orús. A practical introduction to tensor networks: Matrix product states and projected entangled pair states. *Ann. Phys.*, 349:117–158, October 2014.
- [49] David Perez-Garcia, Frank Verstraete, J. Ignacio Cirac, and Michael M. Wolf. PEPS as unique ground states of local Hamiltonians. *Quantum Inf. Comput.*, 8:0650–0663, 2008.
- [50] Norbert Schuch, Ignacio Cirac, and David Perez-Garcia. PEPS as ground states: Degeneracy and topology. *Ann. Phys.*, 325:2153–2192, 2010.
- [51] Bill Sutherland. Model for a multicomponent quantum system. *Phys. Rev. B*, 12:3795, 1975.
- [52] A Koga and N Kawakami. Quantum phase transitions in the Shastry-Sutherland model for $\text{SrCu}_2(\text{BO}_3)_2$. *Phys. Rev. Lett.*, 84(19):4461–4464, May 2000.
- [53] Jianwei Yang, Anders W Sandvik, and Ling Wang. Quantum criticality and spin liquid phase in the Shastry-Sutherland model, 2022.
- [54] Michael Hermele, Ying Ran, Patrick A Lee, and Xiaogang Wen. Properties of an algebraic spin liquid on the kagome lattice. *Phys. Rev. B*, 77(22):224413, June 2008.
- [55] P Nikolic and T Senthil. Physics of low-energy singlet states of the kagome lattice quantum Heisenberg antiferromagnet. *Phys. Rev. B*, 68(21):214415, December 2003.
- [56] Hiroki Nakano and Toru Sakai. Magnetization process of kagome-lattice heisenberg antiferromagnet. *J. Phys. Soc. Jpn.*, 79(5):053707, 2010.
- [57] Jonathan D’Emidio, Stefan Wessel, and Frédéric Mila. Reduction of the sign problem near $T = 0$ in quantum Monte Carlo simulations. *Phys. Rev. B*, 102(6):064420, August 2020.